The Impact of Considering State-of-Charge-Dependent Maximum Charging Powers on the Optimal Electric Vehicle Charging Scheduling

Kun Qian, Reza Fachrizal, Joakim Munkhammar, Thomas Ebel, *Senior Member, IEEE*, and Rebecca C. Adam

***Abstract*— Intelligent charging solutions facilitate mobility electrification. Mathematically, electric vehicle (EV) charging scheduling formulations are constrained optimization problems. Therefore, accurate constraint modeling is theoretically and practically relevant for scheduling. However, the current scheduling literature lacks an accurate problem formulation, including the joint modeling of the nonlinear battery charging profile and minimum charging power constraints. The minimum charging power constraint prevents allocating inexecutable charging profiles. Furthermore, if the problem formulation does not consider the battery charging profile, the scheduling execution may deviate from the allocated charging profile. An insignificant deviation indicates that simplified modeling is acceptable. After providing the problem formulation targeting the maximum possible vehicle battery state-of-charge (SoC) on departure, the numerical assessment shows how the constraint consideration impacts the scheduling performance in typical charging scenarios (weekday workplace and weekend public charging where the grid supplies up to 40 vehicles). The simulation results show that the nonlinear battery charging constraint is practically negligible: For many connected EVs, the grid limit frequently overrules that constraint. The resulting difference between the final mean SoCs using and not using accurate modeling does not exceed 0.2%. Consequently, the results justify simplified modeling (excluding the nonlinear charging profile) for similar scenarios in future contributions.**

***Index Terms*— Charging profile, electric vehicle (EV) charging, minimum charging power, public charging, workplace charging.**

I. Introduction

THE rapidly developing transformation targeting vehicle electrification requires intelligent charging solutions, especially for those infrastructures with limited supply power. One example is workplace charging (supported by more and more companies to promote transportation electrification), where the grid supply power constrains the total charging power. The challenge to charging a group of electric vehicles (EVs) with a constrained grid power is to ensure the fair share of the supply energy and maximize the delivered energy to the EVs, i.e., drivers' satisfaction maximization [1].

The existing smart charging literature covers many aspects, such as the optimization algorithms (mathematical optimization techniques [2] or heuristic optimization approaches [3]) and the strategies (online [4] or offline [5]). The works [6], [7], [8], [9], [10] provide recent reviews on these topics. Related papers often have relaxations on the charging power constraint when they provide problem formulations.

In a practical charging process, apart from the fixed upper bound on the charging power, there is a minimum charging power constraint due to the higher power loss at low charging powers [11]. According to [12], a charging current less than 6 A is not permitted. Ignoring the lower bound in the problem formulation can lead to inexecutable charging profiles, in which case the EVs will not charge. Furthermore, an accurate problem formulation requires a constraint considering that the maximum charging power depends on the increasing state-of-charge (SoC) [1], [13], [14], [15]. Considering these practical constraints is theoretically mandatory to accurately model the charging scheduling problem.

TABLE I
CONSTRAINTS CONSIDERED BY RELATED WORK

		infrastructure-dependent minimum charging power modeled	
		no	yes
SoC-dependent profile modeled	no	[4, 16–22]	[23–28]
	yes	[14, 15, 29–32]	[1]

A. Related Work

The existing EV charging scheduling solutions often assume a relaxation on the minimum charging power, the SoC-dependent maximum charging power, or both the constraints. Table I summarizes how the related contributions combine the four resulting constraint modeling options. Note that only [1] models the combination of both the constraints.

Manuscript received 17 October 2022; revised 29 January 2023; accepted 12 February 2023. Date of publication 14 February 2023; date of current version 13 September 2023. This work was supported in part by the IE Industrial Elektronik Project which has received European Union co-financing from the European Social Fund under Grant SFD-17-0036 and in part by the Swedish Strategic Research Program STandUP for Energy. *(Corresponding author: Kun Qian.)*

Kun Qian, Thomas Ebel, and Rebecca C. Adam are with the Centre for Industrial Electronics (CIE), Department of Mechanical and Electrical Engineering, University of Southern Denmark, DK-6400 Sønderborg, Denmark (e-mail: kqian@sdu.dk; ebel@sdu.dk; rebeccaadam@sdu.dk).

Reza Fachrizal and Joakim Munkhammar are with the Built Environment Energy Systems Group (BEESG), Division of Civil Engineering and Built Environment, Department of Civil and Industrial Engineering, Uppsala University, SE-751 21 Uppsala, Sweden (e-mail: reza.fachrizal@angstrom.uu.se; joakim.munkhammar@angstrom.uu.se).

Digital Object Identifier 10.1109/TTE.2023.3245332

Casini et al. [4] formulated the scheduling problem to minimize the overall daily peak power while satisfying the required energy from the EV users. They developed two real-time algorithms to handle the uncertainties, one using the prior knowledge (statistics of the historical data) while the other not, and they showed the effectiveness via numerical simulations and comparisons. Gan et al. [18] also presented real-time scheduling algorithms for a similar objective, though their decentralized algorithms have advantages such as scalability. However, both the papers applied a continuous charging power range starting from 0 to express the constraint on the charging power. The generated charging profile from the scheduling algorithm can potentially be inexecutable to the charging stations if the charging powers fall below the minimum value. Similarly, this can happen in all the literature categorized in the same group above (some literature starts from a negative value since they consider discharging). Instead of investigating the practical minimum charging power constraint, the existing literature often focuses on studying other aspects of smart charging scheduling (e.g., control architecture [21], [33], control methods [18], [34], and uncertainty handling [35], [36]). To tackle the impracticality, Uiterkamp et al. [23] presented an efficient scheduling algorithm that allows only charging above a given minimum threshold. Zdunek et al. [37], in their modeling, included binary variables to indicate whether the EV is charging or not, which can potentially include the minimum charging power in modeling. Besides traditional modeling, recent literature has successfully applied model-free reinforcement learning (RL) to EV smart charging, where the action space of the RL agent often avoids charging power allocation below the minimum charging power. Sadeghianpourhamami et al. [24] applied RL to schedule the charging of a group of EVs. Their state encapsulates the timing information, the required charging time, and the parking time for those connected EVs. Suited to the state information, the action space consists of selections of different EVs to charge. For charging, they assumed a constant power during the charging process, and consequently, the charging power would never be below the infrastructure-dependent minimum charging power. Tuchnitz et al. [26] discretized the charging power into no charging, charging at half power, and charging at full power, with the possibility of having other intermediate charging levels but avoiding charging levels lower than the minimum charging power. Nevertheless, the contributions above have not studied the effects of the SoC-dependent maximum charging power, whereas, in reality, EVs have variable maximum charging powers dependent on their current SoC [31]. Aziz and Oda [38] presented how the temperature affects the relationship between the charging rate and the SoC. The maximum charging power is constant when the SoC is low in a mild-temperature environment. Two scheduling strategies forbid the executed and the planned schedules from deviating: The first option is to keep the SoC level low. Keeping the SoC level low will not only circumvent the varying maximum charging power but also extend the battery lifetime [39]. However, sometimes it is expected to charge the EVs as much as possible (e.g., to sufficiently cover the next trip). The second option is to consider the SoC-dependent maximum charging power in the problem formulation. Cao et al. [29] showed a nonlinear relationship between the maximum charging power and the SoC to formulate the maximum charging powers over the full SoC range. They take it into account in their rule-based EV charging scheduling. Similarly, Korolko and Sahinoglu [32] considered a smooth curve representing the relationship. They developed a cutting plane algorithm to solve the nonlinear optimization problem by solving a sequence of linear programming problems. Morstyn et al. [15] considered the nonlinear charging profile by applying the equivalent circuit model (ECM) to describe the battery charging. Furthermore, they proposed a reduced-order model which gives approximately the same form of curves as the complex model. El-Bayeh et al. [14] provided a unified mathematical expression where the parameters can change and thus can be used to approximate different battery models. However, they ignored the infrastructure-dependent minimum charging power constraint when formulating the problem. Frendo et al. [1], on the other hand, trained a regression model to predict the maximum charging powers from the historical charging processes. Even though they did not explicitly include the infrastructure-dependent minimum charging power constraint, the model training process should recognize that historically, the EVs never charged below the minimum charging power. However, their rule-based heuristic solution is not optimal, and the impact on optimal scheduling is not studied.

B. Knowledge Gap in EV Charging Scheduling

To directly apply the scheduling computation results and achieve the expected objective, modeling should consider electrical engineering constraints accurately. Ignoring the minimum charging power constraint will potentially lead to inexecutable charging profiles. Thus, this constraint should always be addressed in the problem formulation. Ignoring the SoC-dependent maximum charging power may result in deviation during scheduling execution. As summarized in Table I, most of the existing literature failed to include the minimum charging power constraint when they provided problem formulation considering the SoC-dependent maximum charging power. How considering both the constraints impacts the optimal scheduling performance requires an exploration. Particularly the following questions are currently open.

1) What is the accurate problem formulation for optimizing smart charging given practical electrical engineering constraints?
2) How significant is the deviation between the formulation considering and not considering the SoC-dependent maximum charging power constraint?
3) How to systematically choose the appropriate model given the deviation?

C. Novel Contributions

This article complements the existing smart EV charging literature by the following.

1) The detailed optimal EV charging scheduling formulation considering both the infrastructure-dependent mini-

TABLE II
NOMENCLATURE FOR BATTERY MODELING

Symbol	Description
a_v	battery cell model coefficient, (in $\mathrm{mV/Wh}$)
b_v	battery cell model coefficient, (in V)
E_{norm}	Battery cell nominal energy
i_{t}	Battery cell charging current
$i_{\mathrm{t},k}$	Battery cell charging current at time k
i_{b}	Battery charging current
$i_{\mathrm{b},k}$	Battery charging current at time k
k_0	Charging starting time index
k	Time index
l^0	Initial SoC before charging
M_{p}	Number of cells in parallel
M_{s}	Number of cells in series
$p_{\mathrm{ac},k}$	Real supplied power at time k
Q_{nom}	Nominal battery cell capacity
R	Battery cell impedance
$R\mathrm{eq}$	Battery impedance
v_{t}	Battery cell terminal voltage
$v_{\mathrm{t},k}$	Battery cell terminal voltage at time k
v_{oc}	Battery cell open-circuit voltage
$v_{\mathrm{oc},k}$	Battery cell open-circuit voltage at time k
v_{b}	Battery terminal voltage
$v_{\mathrm{oc_{eq}}}$	Battery open-circuit voltage
V_{max}	Maximum battery cell voltage
η	Charging efficiency

TABLE III
NOMENCLATURE FOR CHARGING SCHEDULING FORMULATION

Symbol	Description
$\mathbf{A}_{\mathrm{load}}$	Auxiliary matrix to compute the load
$\mathbf{A}_{\mathrm{energy}}$	Auxiliary matrix to compute the charged power
$\mathbf{c}_n$	nth EV's connection status
$\mathbf{c}$	Connection status for all EVs
E_{bat}	Battery capacity
e_n	nth EV's energy demand
$\mathbf{e}$	Energy demands for all EVs
H	Scheduling horizon
K	Number of time slots
k	Time index
l_n^0	nth EV's initial SoC
$l_n(k)$	nth EV's SoC at time k
l_{max}	Maximum SoC
N	Number of EVs
$\mathbf{p}_n$	nth EV's charging schedule
$\mathbf{p}$	Charging schedule for all EVs
$\mathbf{p}_{\mathrm{ideal}}$	Result from the ideal formulation
$\mathbf{p}_{\mathrm{realistic}}$	Refined result from $\mathbf{p}_{\mathrm{ideal}}$
$\mathbf{p}_{\mathrm{SoC\text{-}dependent}}$	Result from the SoC-dependent formulation
P_{min}	Minimum charging power
P_{max}	Maximum charging power
P_{grid}	Maximum combined charging power
$\mathbf{s}$	Binary decision variables
T	Decision time slot duration
t_n^{a}	nth EV's arrival time
$\mathbf{t}^{\mathrm{a}}$	Arrival times for all EVs
t_n^{d}	nth EV's departure time
$\mathbf{t}^{\mathrm{d}}$	Departure times for all EVs
η	Charging efficiency

mum charging power and the SoC-dependent maximum charging power.

2) Providing a method to evaluate scheduling deviation in simplified modeling.
3) Providing a systematic modeling workflow for future studies.
4) Concluding whether neglecting the SoC-dependent maximum power constraint constitutes a suitable simplified model in typical charging scenarios.

The optimization objective is to maximize the drivers' satisfaction, i.e., to ensure the fair share of the supply energy and maximize the delivered energy to the EVs. Without loss of generality, the same approach is potentially applicable for exploring other objectives and justifying whether it is necessary to consider the SoC-dependent maximum charging power constraint.

D. Notational Conventions, Nomenclature, and Article Structure

In this article, lowercase boldfaced letters denote vectors. Furthermore, let $\odot$ denote the elementwise product, $\otimes$ denote the Kronecker product, $\preceq$ denote elementwise smaller than and equal to, $\succeq$ denote elementwise greater than and equal to, and $||\bullet||$ denote the Euclidean norm. To ease the reference, the nomenclature in this article is summarized separately in Tables II and III for battery modeling and charging scheduling formulation, respectively.

The remainder of this article is structured as follows. Section II provides the battery model and the computational details for battery charging under the nonlinear charging profile. Section III provides detailed mathematical formulations and important details for scheduling implementation. Section IV first presents the battery charging process simulation and then describes the scheduling simulation scenarios.

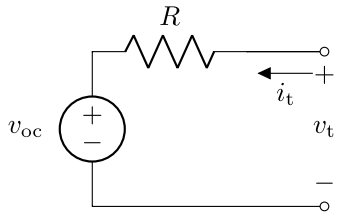

Fig. 1. Battery cell model.

Section V presents the scheduling simulation and its analysis. Finally, Section VI presents the discussion, and Section VII concludes the work.

II. SOC-DEPENDENT MAXIMUM CHARGING POWER

Formulating the SoC-dependent maximum charging power requires modeling the battery charging process. The electrical circuit models (ECMs) can simulate the battery charging process with networks of electrical components such as voltage sources and resistors [40], [41]. Fig. 1 shows a simple battery ECM consisting of a controlled voltage source in serial with an internal resistor [13], [15], [40], [41], where v_{oc} is the open-circuit voltage (OCV), R is the impedance, i_{t} is the charging current, and v_{t} indicates the terminal voltage. Arranging the battery cells in $M_{\mathrm{p}} \times M_{\mathrm{s}}$, where M_{p} and M_{s} denote the number of cells in parallel and series, respectively, yields an equivalent model for the battery, as shown in Fig. 2. Here $v_{\mathrm{oc_{eq}}}$ is the battery OCV, R_{eq} is the impedance, i_{b} is the battery charging current, v_{b} indicates the terminal voltage for the battery, and p_{ac} is the charging power provided by the charging station. Due to the parallel and series arrangement

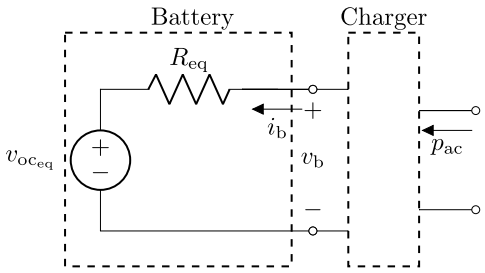

Fig. 2. Battery model.

of the cells, these parameters read

$$v_{\text{b}} = M_{\text{s}} v_{\text{t}} \tag{1}$$

$$v_{\text{oc}_{\text{eq}}} = M_{\text{s}} v_{\text{oc}} \tag{2}$$

$$i_{\text{b}} = M_{\text{p}} i_{\text{t}} \tag{3}$$

$$R_{\text{eq}} = M_{\text{s}} R / M_{\text{p}}. \tag{4}$$

Furthermore, this article uses the linear model from [15] to express the battery cell's OCV v_{oc} depending on the stored energy (neglecting the battery efficiency during charging) at the time index k

$$v_{\text{oc},k} = a_{\text{v}} \underbrace{\left(l^0 E_{\text{nom}} + \tau \sum_{\kappa=k_0}^{k-1} v_{\text{t},\kappa} i_{\text{t},\kappa} \right)}_{\text{stored energy until time index k-1}} + b_{\text{v}} \tag{5}$$

where l^0 is the SoC at the arrival time (AT) index k_0, E_{nom} is the battery cell's nominal energy, τ is the time slot duration, and a_{v} measured in mV/Wh and b_{v} measured in V are the model coefficients.

Battery charging commonly starts with either constant current or constant power and ends with constant voltage (CC-CV or CP-CV). Currently, most EV chargers lead to a CC-CV charging process [42], [43], [44]. However, with the increasing battery voltage during the charging process, the CC-CV scheme results in varying maximum power demands, with a peak power demand at the turning point from the CC mode to CV mode. This is challenging since charging stations usually have a fixed maximum power limit. Instead, the CP-CV charging scheme ensures that the battery charges with constant power until the battery reaches the maximum voltage.

Under the CP-CV charging scheme, the battery is charging with a constant power, when the terminal voltage v_{t} is less than the maximum cell voltage $V_{\max}$ at time index k, and the terminal voltage and the battery charging current read

$$v_{\text{b},k} = v_{\text{oc}_{\text{eq}},k} + R_{\text{eq}} i_{\text{b},k} \tag{6}$$

$$i_{\text{b},k} v_{\text{b},k} = \eta p_{\text{ac},k}. \tag{7}$$

Following the derivation in Appendix in turn determines $v_{\text{b},k}$

$$v_{\text{b},k} = \frac{v_{\text{oc}_{\text{eq}},k}}{2} + \sqrt{\eta p_{\text{ac},k} R_{\text{eq}} + \frac{1}{4} v^2_{\text{oc}_{\text{eq}},k}}. \tag{8}$$

Substituting (8) in (1) and (7) in (3) and rearranging the equations yields $v_{\text{t},k}$ and $i_{\text{t},k}$, respectively, and allows to update the stored energy in each cell at the end of time index k.

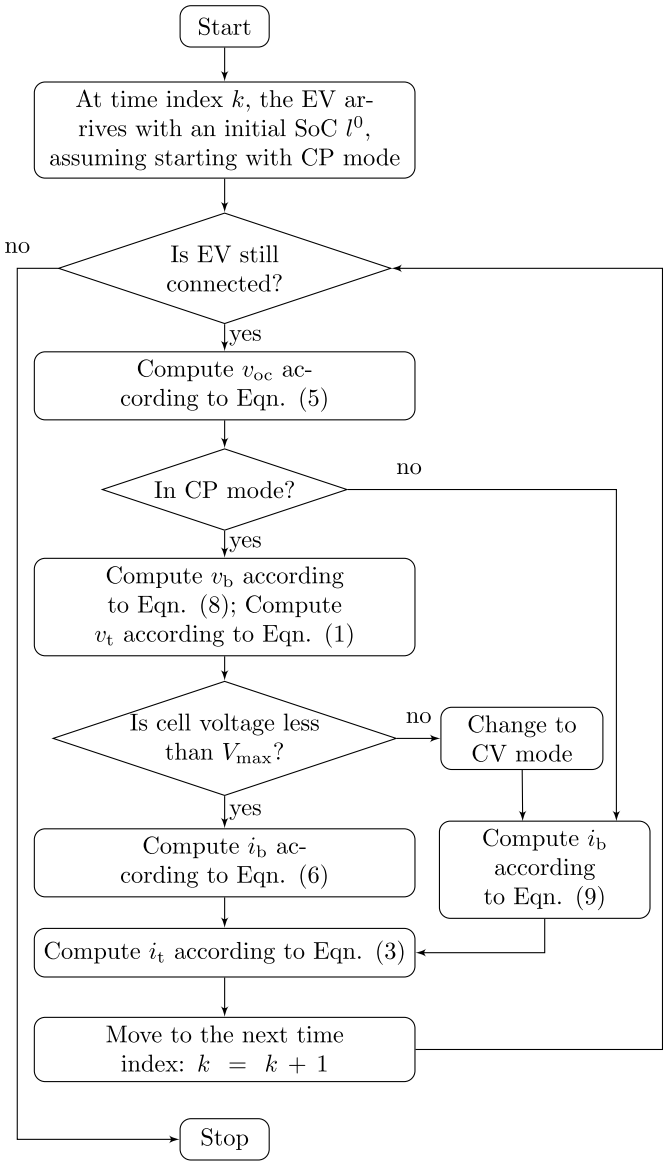

Fig. 3. Flowchart of computing the parameters when charging the battery under the CP-CV scheme.

If the determined v_{t} exceeds $V_{\max}$, the battery is charging with constant voltage, i.e., $v_{\text{t}} = V_{\max}$. Then the battery charging current reads

$$i_{\text{b},k} = \frac{M_{\text{s}} V_{\max} - v_{\text{oc}_{\text{eq}},k}}{R_{\text{eq}}}. \tag{9}$$

Substituting (9) yields the battery cell charging current i_{t} according to (3). The recursive CP-CV battery charging process requires the following steps as shown in Fig. 3.

1) Calculate v_{oc} and v_{t}.
2) Determine the operation mode (CP or CV).
3) Calculate mode-dependent i_{t} and SoC.

Then according to (5), the SoC determines the OCV v_{oc}. Afterward, substituting the OCV in (6) yields the battery cell voltage v_{t}, which indicates the battery charging mode. Note that when the charging station allocates a charging power to the EV, the EV can only take it when charging in the CP mode. If battery charging has moved to the CV mode at time index

k, the real supplied power $p_{\mathrm{ac},k}$ by the charging station reads

$$p_{\mathrm{ac},k} = M_{\mathrm{s}} V_{\max} i_{\mathrm{b},k}/\eta. \tag{10}$$

Consequently, the real charging powers depend on the SoC.

III. Problem Formulation

This section provides a detailed formulation for the optimal EV charging scheduling and covers all the three relevant cases.

1) *Ideal Profile:* The SoC-dependent maximum charging power constraint is not considered in this problem formulation. The ideal profile provides an upper bound for the final mean SoC. This article uses the ideal profile to systematically choose appropriate modeling by examining the deviation between the ideal and realistic profiles.
2) *Realistic Profile:* This article dubs the profile gained by limiting the ideal allocated powers in a second step by the SoC-dependent maximum charging power as the realistic profile.
3) *SoC-Dependent Profile:* The SoC-dependent profile determines the charging power profile gained by directly allocating powers constrained by the SoC-depending maximum charging powers. Therefore, the SoC-dependent profile constitutes both the optimal and realistic performance.

Let N represent the number of charging stations. Furthermore, let H represent the scheduling horizon, T the decision time slot duration, and $K = \lfloor H/T \rfloor$ the total number of time slots.

For the charging behavior, let t_n^{a}, t_n^{d}, l_n^0, and e_n represent the nth EV's AT, departure time (DT), the initial SoC, and energy demand (ED) for all the nodes $n \in \{1, \ldots, N\}$, respectively. This work assumes homogeneous (of the same characteristics) EVs. Let $P_{\min}$, $P_{\max}$, E_{bat}, and $l_{\max}$ represent the minimum, maximum charging power, battery energy, and maximum SoC, respectively. Thus, $e_n = (l_{\max} - l_n^0)E_{\mathrm{bat}}$. The vector $\mathbf{p}_n = [p_n(1), \ldots, p_n(K)]^{\mathsf{T}} \in \mathbb{R}_{\geq 0}^{K\times 1}$ describes the charging schedule for EV $n \in \{1, \ldots, N\}$. Furthermore, η denotes the charging efficiency. The charging schedule depends on the EV connection status. For all EVs $n \in \{1, \ldots, N\}$, the binary connection status vector reads $\mathbf{c}_n = [c_n(1), \ldots, c_n(K)]^{\mathsf{T}} \in \mathbb{B}^{K\times 1}$, with kth ($k \in \{1, \ldots, K\}$) entry

$$c_n(k) = \begin{cases} 1, & \text{if } t_n^{\mathrm{a}} \leqslant kT \leqslant t_n^{\mathrm{d}} \\ 0, & \text{else.} \end{cases} \tag{11}$$

This article presents an implementation-friendly and hence convenient matrix–vector notation by stacking the charging powers in $\mathbf{p} = [\mathbf{p}_1^{\mathsf{T}}, \ldots, \mathbf{p}_N^{\mathsf{T}}]^{\mathsf{T}} \in \mathbb{R}_{\geq 0}^{NK\times 1}$, and the connection time vectors and EDs (ATs, DTs, and EDs) in $\mathbf{c} = [\mathbf{c}_1^{\mathsf{T}}, \ldots, \mathbf{c}_N^{\mathsf{T}}]^{\mathsf{T}}$, $\mathbf{t}^{\mathrm{a}} = [t_1^{\mathrm{a}}, \ldots, t_N^{\mathrm{a}}]^{\mathsf{T}}$, $\mathbf{t}^{\mathrm{d}} = [t_1^{\mathrm{d}}, \ldots, t_N^{\mathrm{d}}]^{\mathsf{T}}$, and $\mathbf{e} = [e_1, \ldots, e_N]^{\mathsf{T}}$, respectively.

To express the summations over the changing schedules $\mathbf{p}_n$ for all $n \in \{1, \ldots, N\}$ as a vector containing the total load at each time index $k \in \{1, \ldots, K\}$

$$\mathbf{A}_{\mathrm{load}}\mathbf{p} = \left[\sum_{n=1}^{N} p_n(1), \ldots, \sum_{n=1}^{N} p_n(K)\right]^{\mathsf{T}} \tag{12}$$

this article uses the auxiliary matrix $\mathbf{A}_{\mathrm{load}} \in \mathbb{R}_{\geq 0}^{K\times NK}$ as follows:

$$\mathbf{A}_{\mathrm{load}} = \mathbf{1}_{1\times N} \otimes \mathbf{I}_K. \tag{13}$$

Similarly the auxiliary matrix $\mathbf{A}_{\mathrm{energy}} \in \mathbb{R}_{\geq 0}^{N\times NK}$

$$\mathbf{A}_{\mathrm{energy}} = \eta T \mathbf{I}_N \otimes \mathbf{1}_{1\times K} \tag{14}$$

expresses the summations over the charging schedules $p_n(k)$ for all $k \in \{1, \ldots, K\}$ and for each $n \in \{1, \ldots, N\}$ as follows:

$$\mathbf{A}_{\mathrm{energy}}\mathbf{p} = \left[\eta T \sum_{k=1}^{K} p_1(k), \ldots, \eta T \sum_{k=1}^{K} p_N(k)\right]^{\mathsf{T}}. \tag{15}$$

This vector contains the total charged energy for each $n \in \{1, \ldots, N\}$.

This article targets maximizing EV driver satisfaction in terms of SoC on departure. Therefore, here the objective is to minimize the difference between the total charged energy and the EDs. To reach the maximum SoC, upon EV's arrival, the required energy is the desired energy. Thus, the objective function for the optimization problem is

$$f(\mathbf{p}) = \|\mathbf{A}_{\mathrm{energy}}\mathbf{p} - \mathbf{e}\|^2. \tag{16}$$

A. Ideal Profile

The ideal profile scenario does not consider the SoC-dependent maximum charging powers. Thus, there are three types of constraints to consider.

1) EVs can either not charge ($= 0$) or charge within a defined power range ($\in [P_{\min}, P_{\max}]$) when connected.
2) At each decision time slot, the total charging power allocated to EVs should be bounded within the grid limit.
3) EVs can, at maximum, acquire the energy that equals their EDs.

Constraint (a) means that the decision variables are bounded in two disjoint ranges, i.e., either 0 or in the range $[P_{\min}, P_{\max}]$. Similar to [37], this article uses extra binary decision variable $\mathbf{s} \in \mathbb{B}^{NK\times 1}$ to constrain charging power variables by the following equation:

$$\mathbf{p} \succeq P_{\min}\mathbf{c} \odot \mathbf{s} \tag{17a}$$

$$\mathbf{p} \preceq P_{\max}\mathbf{c} \odot \mathbf{s}. \tag{17b}$$

For constraint (b), let P_{grid} denote the grid limit

$$\mathbf{A}_{\mathrm{load}}\mathbf{p} \preceq P_{\mathrm{grid}}\mathbf{1}_{K\times 1}. \tag{18}$$

Similarly, constraint (c) uses the auxiliary matrix $\mathbf{A}_{\mathrm{energy}}$

$$\mathbf{A}_{\mathrm{energy}}\mathbf{p} \preceq \mathbf{e}. \tag{19}$$

Consequently, the optimization formulation to compute the "ideal profile," $\mathbf{p}_{\mathrm{ideal}}$, is

$$\mathbf{p}_{\mathrm{ideal}} = \arg\min_{\mathbf{p}} f(\mathbf{p}) \quad \text{s.t.} \begin{cases} P_{\min}\mathbf{c} \odot \mathbf{s} \preceq \mathbf{p} \preceq P_{\max}\mathbf{c} \odot \mathbf{s} \\ \mathbf{A}_{\mathrm{load}}\mathbf{p} \preceq P_{\mathrm{grid}}\mathbf{1}_{K\times 1} \\ \mathbf{A}_{\mathrm{energy}}\mathbf{p} \preceq \mathbf{e}. \end{cases} \tag{20}$$

B. Realistic Profile

Let $l_n(k)$ denote the accumulated SoC until time index $k-1$. Due to the maximum charging power SoC dependency, the actual charging power may deviate from the allocated charging profile. To take this possible deviation into account, the k,nth entry ($\forall k \in \{1,\dots,K\}$ and $\forall n \in \{1,\dots,N\}$) of the realistic power profile vector $\mathbf{p}_{\text{realistic}}$ always determines the minimum value between the ideal profile values and the SoC-dependent maximum charging power $p_{\text{ac,n}}(k)$

$$p_{\text{realistic},n}(k) = \min\big(p_{\text{ideal},n}(k),\, p_{\text{ac,n}}(k)\big). \tag{21}$$

With (21), the accumulated SoC up to time index $k-1$ is

$$l_n(k) = l_n^0 + \frac{\eta T}{E_{\text{bat}}} \sum_{\kappa=1}^{k-1} p_{\text{realistic},n}(\kappa)\,). \tag{22}$$

Following the derivation in Appendix, the SoC-dependent maximum charging power in the CV operation mode reads

$$\begin{aligned} p_{\text{ac},n}(k) &= \underbrace{\frac{M_{\text{s}}^2 V_{\max}}{R_{\text{eq}}\eta}\big(V_{\max} - b_{\text{v}} - a_{\text{v}} E_{\text{nom}} l_n^0\big)}_{\text{denoted as } \alpha_n} \\ &\quad - \underbrace{\frac{M_{\text{s}}^2 a_{\text{v}} E_{\text{nom}} T V_{\max}}{R_{\text{eq}} E_{\text{bat}}}}_{\text{denoted as } \beta} \sum_{\kappa=1}^{k-1} p_{\text{realistic},n}(\kappa) \\ &= \alpha_n - \beta \sum_{\kappa}^{k-1} p_{\text{realistic},n}(\kappa) \end{aligned} \tag{23}$$

where α_n and β are constants, and α_n depends on the nth EV's initial SoC.

As a result, upon getting $\mathbf{p}_{\text{ideal}}$, there will be an iterative process going through each time index for each EV and comparing it to $p_{\text{ac},n}(k)$, and the smaller values are indeed the real supplied charging powers, which will be stored as $\mathbf{p}_{\text{realistic}}$.

C. SoC-Dependent Profile

Besides modeling constraints (a)–(c) like in the ideal profile, the formulation to consider the SoC-dependent maximum charging powers requires an additional constraint for nth EV at time index k

$$\begin{aligned} p_n(k) &\leqslant p_{\text{ac},n}(k) \\ &= \alpha_n - \beta \sum_{\kappa}^{k-1} p_n(\kappa). \end{aligned} \tag{24}$$

Note that (24) only forms the accurate maximum charging power limits in the constant voltage mode. Combining (24) and constraint (a) will provide the accurate maximum charging power limits during the whole charging process since $P_{\max}$ will limit the charging power in the constant power mode.

Rearranging (24) and expanding it over the scheduling horizon $\forall k \in \{1,\dots,K\}$ results in

$$\begin{aligned} p_n(1) &\leq \alpha_n \\ \beta p_n(1) + p_n(2) &\leq \alpha_n \\ &\vdots \\ \beta \sum_{k=1}^{K-1} p_n(k) + p_n(K) &\leq \alpha_n \end{aligned}$$

resulting in the following matrix form:

$$\underbrace{\begin{bmatrix} 1 & 0 & \cdots & 0 \\ \beta & 1 & \cdots & 0 \\ \vdots & \vdots & \ddots & \vdots \\ \beta & \beta & \cdots & 1 \end{bmatrix}_{K\times K}}_{\text{denoted as } \boldsymbol{B}} \begin{bmatrix} p_n(1) \\ p_n(2) \\ \vdots \\ p_n(K) \end{bmatrix}_{K\times 1} = \begin{bmatrix} \alpha_n \\ \alpha_n \\ \vdots \\ \alpha_n \end{bmatrix}_{K\times 1} \tag{25}$$

where the matrix $\boldsymbol{B}$'s diagonal elements have the value 1, and its lower left triangular elements have the value β. Stacking N parameters α_n for all EVs in $\boldsymbol{\alpha} = [\alpha_1,\dots,\alpha_N]^{\mathsf{T}}$ and together with (25) can result in a convenient matrix–vector representation for the extra constraint formulation for all EVs over the scheduling horizon

$$(\mathbf{I}_N \otimes \boldsymbol{B})\mathbf{p} \preceq \boldsymbol{\alpha} \otimes \mathbf{1}_{K\times 1}. \tag{26}$$

Consequently, optimization problem formulation to compute the optimal charging schedule considering the SoC-dependent maximum charging powers $\mathbf{p}_{\text{SoC-dependent}}$, referred to as "SoC-dependent profile," reads

$$\begin{aligned} \mathbf{p}_{\text{SoC-dependent}} = \arg\min_{\mathbf{p}}\ & f(\mathbf{p}) \\ \text{s.t.}\ & \begin{cases} P_{\min}\mathbf{c}\odot\mathbf{s} \preceq \mathbf{p} \preceq P_{\max}\mathbf{c}\odot\mathbf{s} \\ \mathbf{A}_{\text{load}}\mathbf{p} \preceq P_{\text{grid}}\mathbf{1}_{K\times 1} \\ \mathbf{A}_{\text{energy}}\mathbf{p} \preceq \mathbf{e} \\ (\mathbf{I}_N \otimes \boldsymbol{B})\mathbf{p} \preceq \boldsymbol{\alpha} \otimes \mathbf{1}_{K\times 1}. \end{cases} \end{aligned} \tag{27}$$

D. Systematic Modeling Workflow

1) Choosing an Appropriate Model: Note that the final mean SoC from the three different profiles is related by the following inequality:

$$\bar{l}_{\text{real}} \leq \bar{l}_{\text{SoC-dependent}} \leq \bar{l}_{\text{ideal}}. \tag{28}$$

The inequality indicates the lower and upper bounds for $\bar{l}_{\text{SoC-dependent}}$. Thus, EV scheduling practitioners can define a threshold ε for the acceptable final SoC deviation and compare it to the deviation between the "ideal" and "realistic" profiles ($\sigma = \bar{l}_{\text{ideal}} - \bar{l}_{\text{real}}$) to decide whether simplified modeling is acceptable

$$\mathbf{p}_{\text{allocated}} = \begin{cases} \mathbf{p}_{\text{ideal}}, & \text{if } \sigma \leq \varepsilon \\ \mathbf{p}_{\text{SoC-dependent}}, & \text{else.} \end{cases} \tag{29}$$

This simple decision rule is shown in Fig. 4.

2) Implementation Details: Note that the matrix–vector representations in (20) and (27) facilitate easy charging profile implementation for $\mathbf{p}_{\text{ideal}}$ and $\mathbf{p}_{\text{SoC-dependent}}$, with CVX [45] and the *MOSEK* solver [46] in MATLAB.

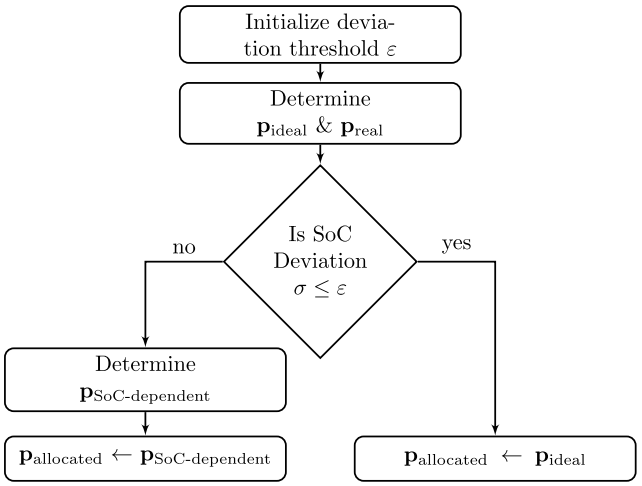

Fig. 4. Simple modeling workflow for practitioners shows that simplified modeling is practically applicable for small final SoC deviations between the "ideal" and "realistic" profiles.

TABLE IV
BATTERY PARAMETERS

Parameters	Descriptions	Values
V_{nom}	nominal cell voltage	3.7 V
V_{max}	maximum cell voltage	4.15 V
R	cell impedance	148 mΩ
Q_{nom}	nominal cell capacity	2.2 A h
E_{nom}	nominal cell energy	8.14 W h
M_{p}	number of cells in parallel	50
M_{s}	number of cells in series	100
a_{v}	model coefficient	67.92 mV/Wh
b_{v}	model coefficient	3.592 V

IV. SIMULATION SETUP

This section first declares and defines the EV battery's relevant parameters, and then shows the charging process simulation. The considered two scenarios (weekday workplace charging and weekend public charging) apply the battery parameters and other relevant parameters. Finally, a discussion on the performance evaluation illuminates the later simulation results.

A. Battery Charging Process

For further simulations, this article uses the battery parameters from [15], as summarized in Table IV. Other parameters summarized in Table V are a prerequisite to simulate the charging process.

Fig. 5 shows the battery charging process simulations based on the parameters from Tables IV and V. In Fig. 5, the charging power stays at the maximum charging power ($P_{\text{ac}}^{\max} = 11.04$ kW) during the constant power charging mode, which is on the left side of the blue dash-dot line. The battery voltage increases while the charging current decreases. The charging mode changes to the constant voltage mode when the battery voltage reaches the maximum value ($M_{\text{s}} V_{\max} = 415$ V), which is indicated by the blue dash-dot line. Then the battery cannot use the maximum charging power anymore. Instead, the used charging power is nonlinearly decreasing over time. Considering the practical minimum charging power ($P_{\text{ac}}^{\min} = 4.14$ kW), the charging process will end earlier, as shown by the dashed lines in Fig. 5. Fig. 6 shows the resulting SoC-dependent maximum charging power, and the dashed line indicates the maximum charging power for the case considering the practical minimum charging power limit.

TABLE V
PARAMETERS FOR BATTERY CHARGING PROCESS SIMULATION

Parameters	Descriptions	Values
V_{ac}	AC voltage at the charging station	230 V
$I_{\text{ac}}^{\max}$	Maximum charging current	16 A
$I_{\text{ac}}^{\min}$	Minimum charging current	6 A
m	Number of phases	3
$P_{\text{ac}}^{\max}$	Maximum charging power	11.04 kW
$P_{\text{ac}}^{\min}$	Minimum charging power	4.14 kW
η	Charging efficiency	0.88
l^0	Initial SoC	0.7
τ	Simulation time slot duration	1 min
T_{sim}	Simulation time period	150 min

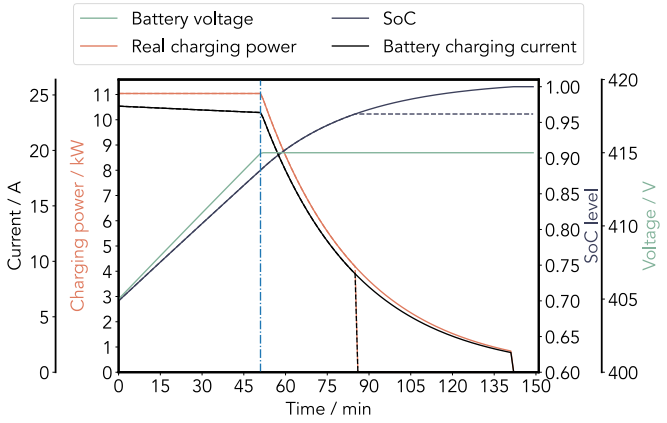

Fig. 5. Battery charging process simulation. The left side of the blue dash-dot line shows the constant power charging mode, and the mode changes to the constant voltage when the battery voltage reaches 415 V, as shown in the right side of the blue dash-dot line. The charging process will end earlier if the model includes the practical minimum charging power, as shown via the dashed lines.

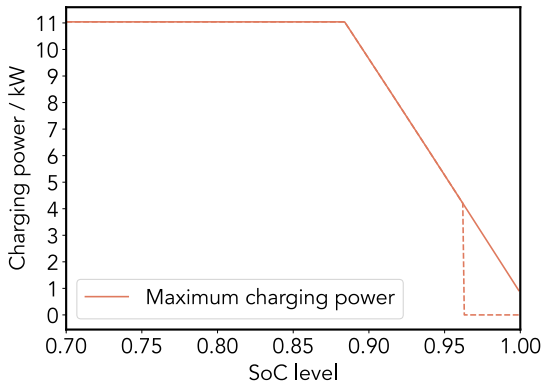

Fig. 6. SoC-dependent maximum charging power. The dashed line indicates that the maximum charging power decreases from 4.14 kW directly to 0 if considering the practical minimum charging power limit.

TABLE VI
COMMON SIMULATION PARAMETERS FOR THE CHARGING SCENARIOS

Parameters	Descriptions	Values
N	Number of EVs	$\{10, 15, 20, 25, 30, 35, 40\}$
E_{bat}	Battery energy	40.7 kWh
$l_{\max}$	Maximum SoC	0.96
$P_{\min}$	Minimum charging power	4.14 kW
$P_{\max}$	Maximum charging power	11.04 kW
P_{grid}	Grid limit	22 kW
η	Charging efficiency	0.88
H	Scheduling horizon	min of ATs - max of DTs
T	Decision time slot duration	15 min
J	Number of simulations	20

B. Simulation Scenarios

The numerical results in this article cover two charging scenarios: weekday workplace charging and weekend public charging. For each charging scenario. First, the decision time slot duration is constant to investigate the results from varying the number of EVs; then, the number of EVs is constant to investigate the results from varying the decision time slot duration. Consequently, this work assesses four simulation scenarios.

For the fixed decision time slot duration, this article chooses the most often used value in the literature: 15 min [7], [47], [48], corresponding to the typical communication time between the energy management units and the grid [49]. The experimental setting chooses the least number of EVs with a proper final average SoC to limit the computational complexity. The final mean SoC should be smaller than the maximum SoC so that there is room for potential improvement by varying the decision time slot duration.

1) Fixed Decision Time Slot Duration: This article first considers a fixed decision time slot duration and varies the number of EVs from 10 to 40, with a step size of 5, and samples the charging behavior from the existing datasets. To compensate for the sampling randomness, this work samples J (here $J = 20$) times for a fixed number of EVs and computes the charging profile. The scheduling horizon extends from the first AT to the last DT. Apart from the different charging behaviors, the two charging scenarios use the same parameters.

There is a fixed maximum grid limit, $P_{\text{grid}} = 22$ kW. Charging stations can supply minimum 4.14 kW ($P_{\min}$, corresponding to three-phase 6 A) and maximum 11.04 kW ($P_{\max}$, corresponding to three-phase 16 A) during the charging process. The charging efficiency, η, is set to 0.88. This work assumes the same battery energy of $E_{\text{bat}} = 40.7$ kWh (a result from Table IV) and a maximum SoC of $l_{\max} = 0.96$ (this value approximates the maximum SoC according to the simulation result shown in Fig. 5).

Table VI summarizes the simulation parameters and their values. In addition, they share the SoC-dependent maximum charging power limit. In this work, the two charging behavior settings are as follows.

Weekday Workplace Charging: Assumes that EVs arrive with an initial SoC of $l(0) = 0.7$, corresponding to an ED of 0.26×40.7 kWh $= 10.58$ kWh (the authors are missing appropriate data to describe the ED, and therefore roughly assumed an ED covering the round trip: workplace–home–workplace.). For the ATs and DTs, this article uses the user mobility data from the Swedish travel survey in 2006 [50], [51]. The arrival and DTs of trips made by cars and other information are available in the survey, and it is considered representative for Scandinavian conditions. Randomly sampling the survey data distributions in a Monte Carlo fashion and assuming that each EV made one round trip (home-work-home) during the weekday yields the ATs and DTs used here. Fig. 7 shows the histogram of the weekday ATs and DTs at the workplace.

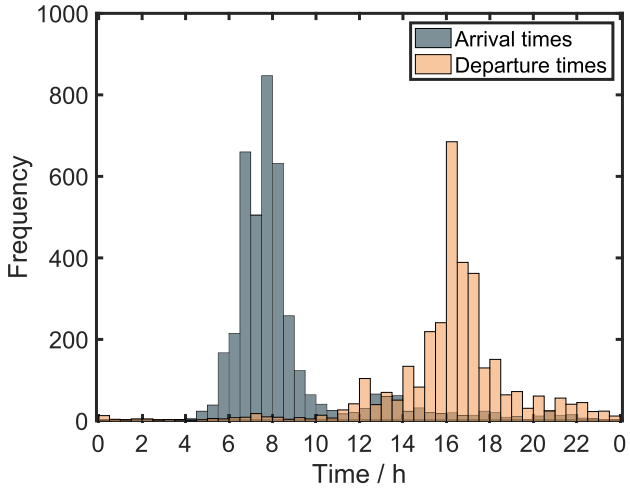

Fig. 7. Histogram of the weekday ATs and DTs at the workplace from the survey data.

Weekend Public Charging: Lahariya et al. [52], based on the real-world EV sessions, have trained statistical models to generate samples of realistic EV charging behavior data which consist of ATs, DTs, and EDs. According to [52], the generated samples are statistically indistinguishable from real-world data. This work used the trained model and generated the charging behavior for the date 20th June 2015 (Saturday). The following postprocessing steps prepared the data used in the simulations.

1) The DTs are limited to a single day.
2) To account for the assumed battery energy of $E_{\text{bat}} = 40.7$ kWh and three-phase charging, this work accordingly tripled the generated EDs.
3) The experimental setup excludes sessions for those the refined EDs exceed the maximum battery energy, for those the refined EDs fall below the minimum ED, and for those the stay duration is not long enough to finish charging.

Fig. 8 shows the histogram of the ATs and DTs, and Fig. 9 shows the histogram of the EDs.

2) Fixed Number of EVs: The result from the above simulation decides how many EVs to include for the next simulation. This setup varies the decision time slot duration from 5 to 30 min, with a step size of 5 min. The other parameters and the charging behavior data are the same as the above simulation scenarios (with fixed decision time slot duration).

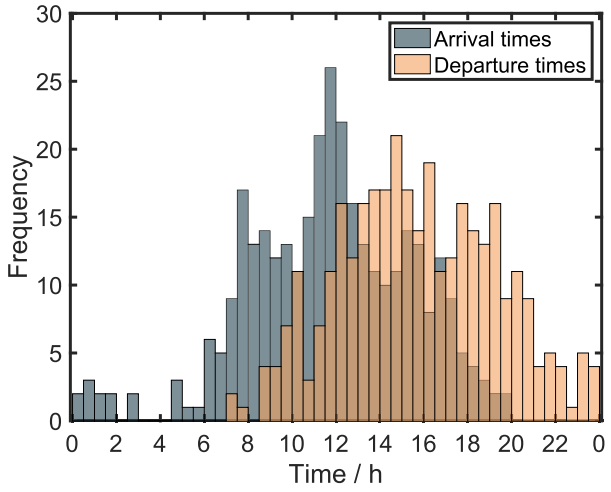

Fig. 8. Histogram of the ATs and DTs for the weekend public charging scenario.

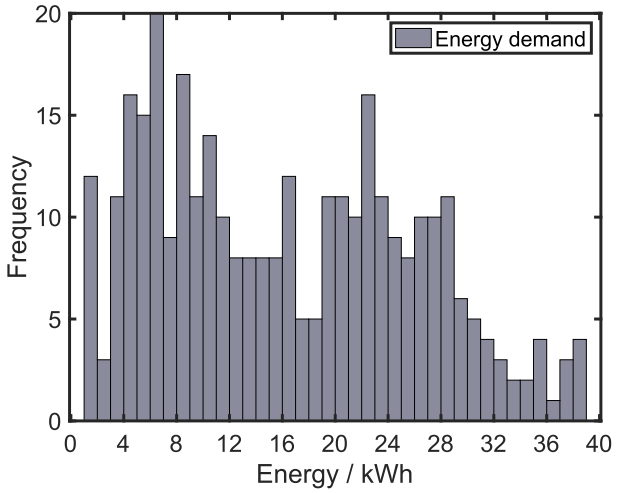

Fig. 9. Histogram of the EDs for the weekend public charging scenario.

C. Performance Evaluation

The scheduling objective is to maximize drivers' satisfaction, i.e., to ensure the fair share of the supply power and maximize the delivered energy to the EVs. The fair share is ensured by the objective function minimizing the difference between the total charged energy and the ED for each EV. This article compares the average mean final SoCs (averaging over 20 simulations for the number of simulated EVs) for the introduced formulations.

V. Simulation Results and Analysis

A. Scheduling Performance Comparison

This work numerically compares the final mean SoCs for scheduling via simplified modeling ("ideal") and for scheduling based on accurate problem formulation including all the constraints ("SoC-dependent"). Note that the "ideal" scheduling formulation calculating $\mathbf{p}_{\text{ideal}}$ covers simplified modeling as formulated in [23] and [37].

Figs. 10 and 11 show comparison of the "realistic profile" mean final SoC (lower bound) to the "ideal profile" mean final SoC (upper bound). The figures only show the "SoC-dependent profile," if there are significant differences between the "realistic profile" and the "ideal profile" following (25). Showing the "SoC-dependent profile" is unnecessary, if there is no visually identifiable difference or only a slight difference.

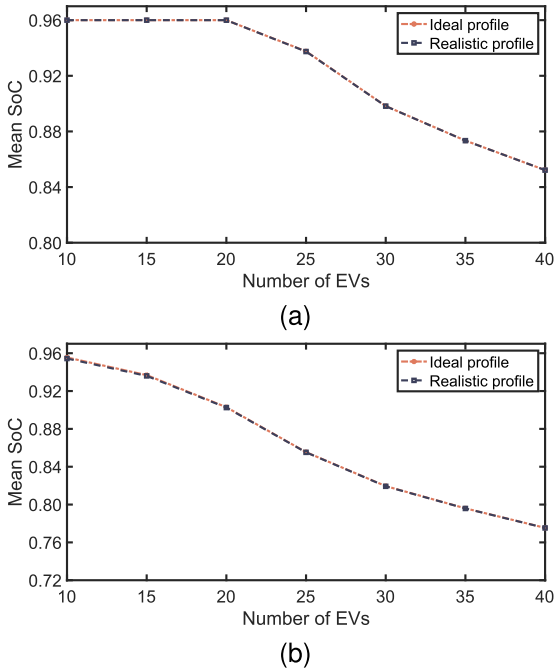

Fig. 10. Average mean final SoC when varying the number of EVs: (a) weekday workplace charging and (b) weekend public charging.

Fig. 10 shows the average mean final SoC when varying the number of EVs. There is an overall decreasing trend with the increasing number of EVs. However, neither Fig. 10(a) nor (b) shows a visually identifiable difference between the "ideal profile" and "realistic profile."

Based on the simulation result, further simulations will have a fixed number of EVs but varying decision time slot duration from 5 to 30 min, with a step size of 5 min. The number of EVs is 25 and 15 for weekday workplace charging and weekend public charging, respectively. Fig. 11 shows the average mean final SoC. Fig. 11 shows a decreasing trend with the increasing decision time slot duration, which confirms the intuition that the average mean final SoC should be higher when the time resolution is higher. Furthermore, there is a slight difference in Fig. 11(a) at 5-min duration for the weekday workplace charging. However, there are significant differences for the weekend public charging at 5 and 10 min duration and a slight difference at 15 min duration, as shown in Fig. 11(b). The EVs cannot always take advantage of the charging power allocated by the charging stations due to the existence of SoC-dependent maximum charging powers in some time slots.

The significant differences for the weekend public charging at 5 and 10 min require further simulating the "SoC-dependent profile" according to (27), and the results are also shown in Fig. 11(b). By considering the SoC-dependent maximum charging power constraint, it is clear that the

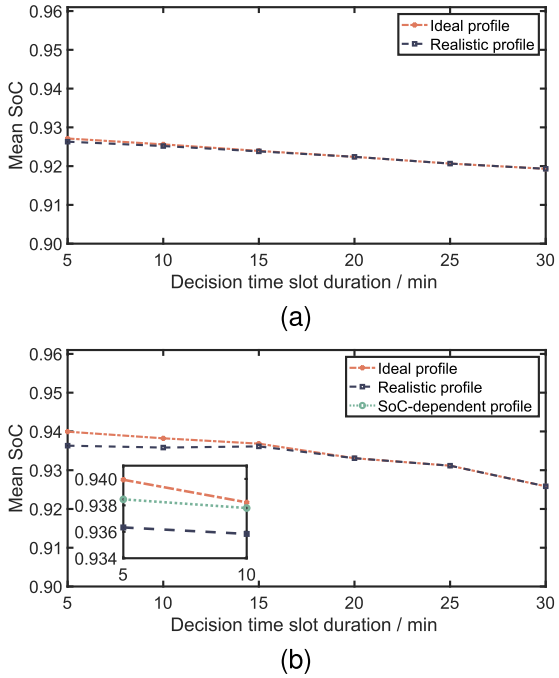

Fig. 11. Average mean final SoC when varying the decision time slot duration: (a) weekday workplace charging and (b) weekend public charging.

"SoC-dependent profile" achieves higher average mean final SoCs compared with the "realistic profile."

B. Example Charging Profile

Fig. 12 shows the example charging profiles, together with the EVs' connection status. As seen from Fig. 12, there are a few time slots when the EVs cannot fully take the allocated charging power by the charging stations, highlighted by the two ellipses. The "realistic profile" is below the "ideal profile" at those time slots. Finally, the "ideal profile" and "realistic profile" have an average mean final SoC at 95.86% and 95.18%, receptively. The "SoC-dependent profile" has a different shape than the "ideal profile," and it achieves an average mean final SoC at 95.72%.

C. Analysis

In both the weekday workplace and weekend public charging simulations, there is no visually identifiable difference between the "ideal profile" and the "realistic profile" with the fixed decision time slot duration at 15 min. The reason is that the simulations start with the number of EVs at 10, and due to the grid limit ($P_{\text{grid}} = 22$ kW), the allocated charging powers are mainly at the lower end. Thus, the SoC-dependent maximum charging power constraint is almost inactive during the scheduling horizon, resulting in nearly no difference. Fig. 13 further demonstrates the reasoning by showing an example charging process for one EV. The vertical dashed lines indicate the arrival and DT for the EV. As shown, the ideal charging powers are consistently below the SoC-dependent maximum charging powers, and consequently, the "realistic profile" will be the same as the "ideal profile." The reason the optimizer allocates small charging powers is that the grid limit P_{grid} is 22 kW while there are many EVs connected. In such cases, the SoC-dependent maximum charging power constraint is overruled by the grid limit, and thus it is never active.

Then, with the fixed number of EVs and varying decision time slot duration, the average mean final SoC is the highest at the duration 5 min. There are two reasons: first, since the generated ATs and DTs are timestamps, a smaller decision time slot duration may result in a longer scheduling horizon (e.g., the scheduling horizon starting point for the EV arriving at 06 : 04 will be 06 : 05 and 06 : 10 for the duration at 5 and 10 min, respectively); second, with a higher resolution, the optimization solver has more options to assign the charging powers, resulting in a potentially higher average mean final SoC. However, a better "ideal profile" does not always ensure a better "realistic profile," as seen from Fig. 11(b). The reason is that when computing the "realistic profile" based on the "ideal profile," the SoC-dependent maximum charging power constraint will become active with the increasing SoC level along the scheduling horizon. To cope with the constraint, the problem formulation requires including it, resulting in the "SoC-dependent profile." The resulting average mean final SoC is higher than the "realistic profile" but still below the "ideal profile" since the "ideal profile" ignores the SoC-dependent maximum charging power constraint when computing the profile. Fig. 14 demonstrates the reasoning by showing an example charging process for one EV. As seen from Fig. 14(a), with the increasing SoC, the SoC-dependent maximum charging power constraint becomes active, and the EV cannot use those allocated powers that exceed the constraint. On the other hand, $\mathbf{p}_{\text{SoC-dependent}}$ ensures that the allocated charging powers are always below the constraint.

Another point worth noting is that the solution from the "ideal profile" is not unique. For example, an EV charging with 4.14 kW first and then 11.04 kW or vice versa would bring the same result according to the objective function. Nevertheless, the former allocation may cause a higher deviation when computing the "realistic profile." The SoC level increases during charging, meaning the maximum charging power will start decreasing at some point. At the beginning of the charging process, the allocation of high charging power has a higher chance of delivering the planned power.

Fig. 11(b) shows the improvement in the average mean final SoC by considering the SoC-dependent maximum charging power constraint. However, the improvement is around 0.2%, which may extend the driving range by approximately 1 km. Compared with the extra 1 km, the saving on the computational resources by excluding the SoC-dependent maximum charging power constraint may be of more interest. Besides, Fig. 10 shows no visually identifiable difference between the "ideal profile" and "realistic profile" with the fixed decision time slot duration at 15 min, which is the most often used value in the literature.

VI. Discussion

This work highlighted two electrical engineering constraints often ignored in EV charging scheduling formulation: the

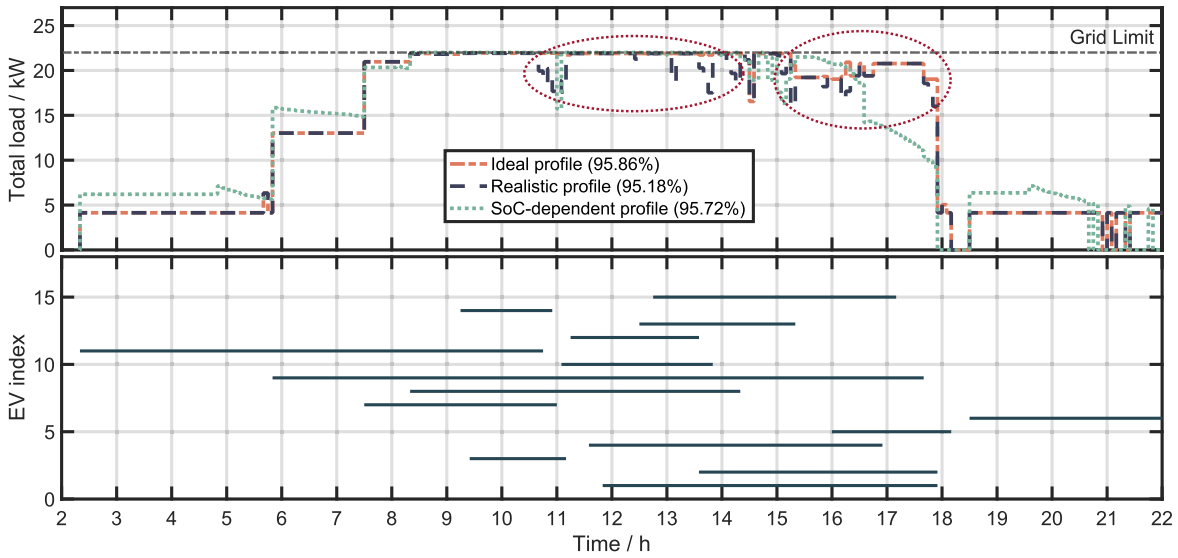

Fig. 12. Example profiles and EVs' connection status from one simulation.

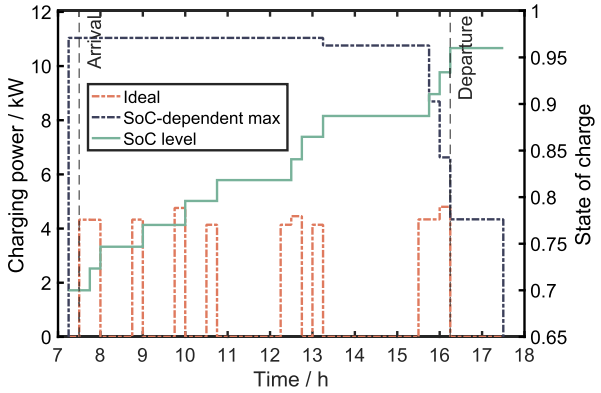

Fig. 13. Example charging process for one EV (the allocated charging powers are always below the SoC-dependent maximum charging powers). "Ideal" shows the allocated charging powers over the scheduling horizon. "SoC level" is the SoC at the beginning of each time index. "SoC-dependent max" shows the SoC-dependent maximum charging powers over the scheduling horizon.

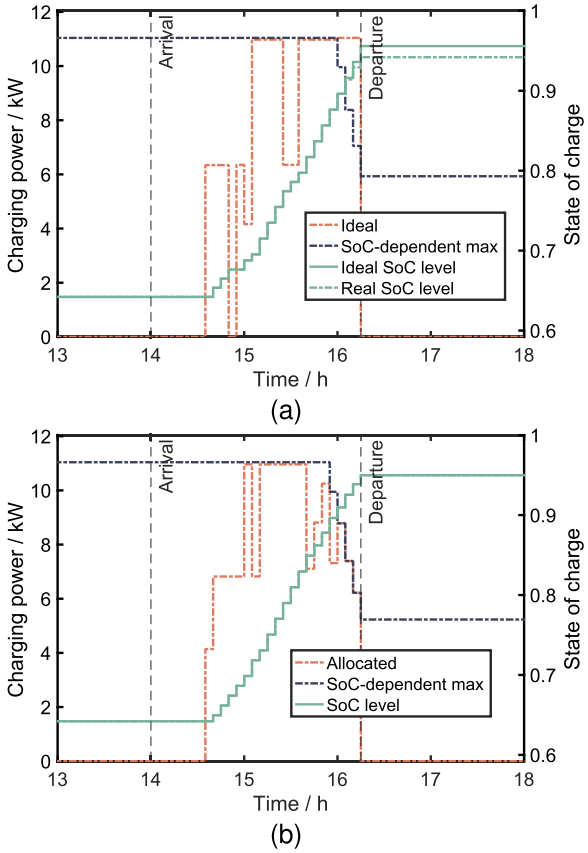

Fig. 14. Example charging process for one EV: (a) computed $\mathbf{p}_{\text{ideal}}$, i.e., ideal charging profile, violates the SoC-dependent maximum charging power constraint, and the final realistic SoC level (94.19%) of this EV is smaller than planned (95.59%) and (b) SoC-dependent maximum charging power constraint is considered when computing $\mathbf{p}_{\text{SoC-dependent}}$, and thus, the allocated powers are always below the constraint, resulting in the SoC level at 94.99%.

infrastructure-dependent minimum charging power and the SoC-dependent maximum charging power. To generate a practically applicable charging scheduling, it is necessary to always include the infrastructure-dependent minimum charging power. As a result, the constraint for the charging power is in two disjoint ranges instead of a continuous range, which leads to the problem falling into the mixed-integer model and slightly increased problem complexity.

As for the SoC-dependent maximum charging power, this article applied the reduced ECM model from [15] for the battery. For simplicity, the proposed method assumed the same battery type for all the EVs considered in the scheduling problem. A more accurate model can potentially compute more practically applicable scheduling. This would further increase the problem's complexity and result in a longer computation time. Thus, evaluating the deviation can provide insight into whether it is necessary to include this constraint in the optimization problem. However, the evaluation still requires modeling the battery charging process. The battery parameters differ from one battery type to another. Besides, other practical aspects such as battery degradation will also affect charging process modeling. One direction for future work is to model the battery charging behavior from the

historical charging processes, which can not only simplify deviation evaluation but also improve the applicability of the accurate model when the deviation is significant.

Section III gradually presented how to compute the ideal, realistic, and SoC-dependent charging profiles. With the defined weekday workplace and weekend public charging scenarios, there are no or only slight deviations when directly applying the ideal profile. Consequently, as proposed in Fig. 4, instead of formulating the problem as in (27), the simpler version as in (20) can be used. Thus, in some existing literature where the SoC-dependent maximum charging powers are not considered, their resulting charging scheduling may be perfectly fine. What they are missing is a justification. Practical applications or future research can also directly take advantage of the result and method from this work to justify their simplified modeling.

The results are valid for the defined simulation scenarios. Nonetheless, the weekday workplace and weekend public charging are typical real-life charging scenarios. The objective, on the other hand, can vary in different studies. In addition, the extra constraint posed by the grid can change. Future studies can further explore the effect of the SoC-dependent maximum charging power constraint in different simulation settings.

VII. Conclusion

This article presents the mathematical formulation for optimal EV charging scheduling considering practical charging power constraints, especially the upper bound depending on the SoC. The simulations show that the scheduling performance increases by taking into account the SoC-dependent maximum charging power constraint with a small decision time slot duration. However, the increased final SoC will not extend the driving range significantly. By setting the decision time slot duration to 15 min, which is the typical value in the literature, there is no deviation when executing the schedule from simplified modeling. Further studies or practical scheduling implementations in a similar situation may exclude the SoC-dependent maximum charging power constraint in their formulation to reduce the complexity.

Appendix

Derivation of Equation (8)

Determining $i_{b,k}$ from (7)

$$i_{b,k} = \eta \frac{p_{\mathrm{ac},k}}{v_{b,k}} \tag{30}$$

and substituting $i_{b,k}$ by (30) in (6) yields

$$v_{b,k} = v_{\mathrm{oc_{eq}}} + R_{\mathrm{eq}} \eta \frac{p_{\mathrm{ac},k}}{v_{b,k}}. \tag{31}$$

Multiplying both sides of (31) with $v_{b,k}$ and rearranging the equation in a way that completing the square can be applied

$$v_{b,k}^2 - v_{\mathrm{oc_{eq}}} v_{b,k} = R_{\mathrm{eq}} \eta p_{\mathrm{ac},k}. \tag{32}$$

Completing the square

$$\left(v_{b,k} - \frac{1}{2} v_{\mathrm{oc_{eq}}}\right)^2 + \frac{1}{4} v_{\mathrm{oc_{eq}}}^2 = R_{\mathrm{eq}} \eta p_{\mathrm{ac},k} + \frac{1}{4} v_{\mathrm{oc_{eq}}}^2. \tag{33}$$

Then it is straightforward that the solution for $v_{b,k}$ is (8)

$$v_{b,k} = +\frac{1}{2} v_{\mathrm{oc_{eq}}} \pm \sqrt{R_{\mathrm{eq}} \eta p_{\mathrm{ac},k} + \frac{1}{4} v_{\mathrm{oc_{eq}}}^2}. \tag{34}$$

Derivation of Equation (23)

First substituting $v_{\mathrm{oc},k}$ calculated in (5) in (9) yields

$$\begin{aligned} i_{\mathrm{b}}(l_n(k)) = {} & \frac{M_{\mathrm{s}}}{R_{\mathrm{eq}}} \left(V_{\max} - b_{\mathrm{v}} - a_{\mathrm{v}} E_{\mathrm{nom}} l_n^0\right) \\ & - \frac{M_{\mathrm{s}} a_{\mathrm{v}} E_{\mathrm{nom}} \eta T}{R_{\mathrm{eq}} E_{\mathrm{bat}}} \sum_{\kappa=1}^{k-1} p_n(\kappa). \end{aligned} \tag{35}$$

Then substituting $i_{b,k}$ calculated in (35) in (10) results in (23)

$$\begin{aligned} p_{\mathrm{ac},n}(k) = {} & \underbrace{\frac{M_{\mathrm{s}}^2 V_{\max}}{R_{\mathrm{eq}} \eta} \left(V_{\max} - b_{\mathrm{v}} - a_{\mathrm{v}} E_{\mathrm{nom}} l_n^0\right)}_{\text{denoted as } \alpha_n} \\ & - \underbrace{\frac{M_{\mathrm{s}}^2 a_{\mathrm{v}} E_{\mathrm{nom}} T V_{\max}}{R_{\mathrm{eq}} E_{\mathrm{bat}}}}_{\text{denoted as } \beta} \sum_{\kappa=1}^{k-1} p_n(\kappa) \\ = {} & \alpha_n - \beta \sum_{\kappa}^{k-1} p_n(\kappa). \end{aligned}$$

References

[1] O. Frendo, J. Graf, N. Gaertner, and H. Stuckenschmidt, "Data-driven smart charging for heterogeneous electric vehicle fleets," *Energy AI*, vol. 1, Aug. 2020, Art. no. 100007. [Online]. Available: https://www.sciencedirect.com/science/article/pii/S2666546820300070

[2] H. Ren et al., "Optimal scheduling of an EV aggregator for demand response considering triple level benefits of three-parties," *Int. J. Electr. Power Energy Syst.*, vol. 125, Feb. 2021, Art. no. 106447. [Online]. Available: https://www.sciencedirect.com/science/article/pii/S0142061519339456

[3] O. Frendo, N. Gaertner, and H. Stuckenschmidt, "Improving smart charging prioritization by predicting electric vehicle departure time," *IEEE Trans. Intell. Transp. Syst.*, vol. 22, no. 10, pp. 6646–6653, Oct. 2021.

[4] M. Casini, A. Vicino, and G. G. Zanvettor, "A receding horizon approach to peak power minimization for EV charging stations in the presence of uncertainty," *Int. J. Electr. Power Energy Syst.*, vol. 126, Mar. 2021, Art. no. 106567.

[5] Z. Liu, Q. Wu, S. Huang, L. Wang, M. Shahidehpour, and Y. Xue, "Optimal day-ahead charging scheduling of electric vehicles through an aggregative game model," *IEEE Trans. Smart Grid*, vol. 9, no. 5, pp. 5173–5184, Sep. 2018.

[6] W. Tang, S. Bi, and Y. J. Zhang, "Online charging scheduling algorithms of electric vehicles in smart grid: An overview," *IEEE Commun. Mag.*, vol. 54, no. 2, pp. 76–83, Dec. 2016.

[7] Q. Wang, X. Liu, J. Du, and F. Kong, "Smart charging for electric vehicles: A survey from the algorithmic perspective," *IEEE Commun. Surveys Tuts.*, vol. 18, no. 2, pp. 1500–1517, 2nd Quart., 2016.

[8] M. Uddin, M. F. Romlie, M. F. Abdullah, S. A. Halim, A. H. A. Bakar, and T. C. Kwang, "A review on peak load shaving strategies," *Renew. Sustain. Energy Rev.*, vol. 82, pp. 3323–3332, Feb. 2018. [Online]. Available: https://www.sciencedirect.com/science/article/pii/S1364032117314272

[9] R. Fachrizal, M. Shepero, D. van der Meer, J. Munkhammar, and J. Widén, "Smart charging of electric vehicles considering photovoltaic power production and electricity consumption: A review," *eTransportation*, vol. 4, May 2020, Art. no. 100056. [Online]. Available: https://www.sciencedirect.com/science/article/pii/S2590116820300138

[10] N. I. Nimalsiri, C. P. Mediwaththe, E. L. Ratnam, M. Shaw, D. B. Smith, and S. K. Halgamuge, "A survey of algorithms for distributed charging control of electric vehicles in smart grid," *IEEE Trans. Intell. Transp. Syst.*, vol. 21, no. 11, pp. 4497–4515, Nov. 2020.

[11] E. Apostolaki-Iosifidou, P. Codani, and W. Kempton, "Measurement of power loss during electric vehicle charging and discharging," *Energy*, vol. 127, pp. 730–742, May 2017.

[12] *Electric Vehicle Conductive Charging System—Part 1: General Requirements*, document IEC 61851-1, International Electrotechnical Commission, 2019.

[13] F. Marra, G. Ya Yang, E. Larsen, C. N. Rasmussen, and S. You, "Demand profile study of battery electric vehicle under different charging options," in *Proc. IEEE Power Energy Soc. Gen. Meeting*, Jul. 2012, pp. 1–7.

[14] C. Z. El-Bayeh, I. Mougharbel, M. Saad, A. Chandra, D. Asber, and S. Lefebvre, "Impact of considering variable battery power profile of electric vehicles on the distribution network," in *Proc. 4th Int. Conf. Renew. Energies Developing Countries (REDEC)*, Nov. 2018, pp. 1–8.

[15] T. Morstyn, C. Crozier, M. Deakin, and M. D. McCulloch, "Conic optimization for electric vehicle station smart charging with battery voltage constraints," *IEEE Trans. Transport. Electrific.*, vol. 6, no. 2, pp. 478–487, Jun. 2020.

[16] Y. He, B. Venkatesh, and L. Guan, "Optimal scheduling for charging and discharging of electric vehicles," *IEEE Trans. Smart Grid*, vol. 3, no. 3, pp. 1095–1105, Sep. 2012.

[17] S. Bashash and H. K. Fathy, "Optimizing demand response of plug-in hybrid electric vehicles using quadratic programming," in *Proc. Amer. Control Conf.*, Jun. 2013, pp. 716–721.

[18] L. Gan, U. Topcu, and S. H. Low, "Optimal decentralized protocol for electric vehicle charging," *IEEE Trans. Power Syst.*, vol. 28, no. 2, pp. 940–951, May 2013.

[19] S. Bashash and H. K. Fathy, "Cost-optimal charging of plug-in hybrid electric vehicles under time-varying electricity price signals," *IEEE Trans. Intell. Transp. Syst.*, vol. 15, no. 5, pp. 1958–1968, Oct. 2014.

[20] L. Zhang, V. Kekatos, and G. B. Giannakis, "Scalable electric vehicle charging protocols," *IEEE Trans. Power Syst.*, vol. 32, no. 2, pp. 1451–1462, Mar. 2017.

[21] R. Wang, G. Xiao, and P. Wang, "Hybrid centralized-decentralized (HCD) charging control of electric vehicles," *IEEE Trans. Veh. Technol.*, vol. 66, no. 8, pp. 6728–6741, Aug. 2017.

[22] K. Qian, R. Brehm, T. Ebel, and R. C. Adam, "Electric vehicle load management: An architecture for heterogeneous nodes," *IEEE Access*, vol. 10, pp. 59748–59758, 2022.

[23] M. H. H. S. Uiterkamp, T. van der Klauw, M. E. T. Gerards, and J. L. Hurink, "Offline and online scheduling of electric vehicle charging with a minimum charging threshold," in *Proc. IEEE Int. Conf. Commun., Control, Comput. Technol. Smart Grids (SmartGridComm)*, Oct. 2018, pp. 1–6.

[24] N. Sadeghianpourhamami, J. Deleu, and C. Develder, "Definition and evaluation of model-free coordination of electrical vehicle charging with reinforcement learning," *IEEE Trans. Smart Grid*, vol. 11, no. 1, pp. 203–214, Jan. 2020.

[25] K. Qian, R. Adam, and R. Brehm, "Reinforcement learning based EV charging scheduling: A novel action space representation," in *Proc. IEEE PES Innov. Smart Grid Technol. Asia (ISGT Asia)*, Dec. 2021, pp. 1–5.

[26] F. Tuchnitz, N. Ebell, J. Schlund, and M. Pruckner, "Development and evaluation of a smart charging strategy for an electric vehicle fleet based on reinforcement learning," *Appl. Energy*, vol. 285, Mar. 2021, Art. no. 116382. [Online]. Available: https://www.sciencedirect.com/science/article/pii/S0306261920317566

[27] J. Lee, E. Lee, and J. Kim, "Electric vehicle charging and discharging algorithm based on reinforcement learning with data-driven approach in dynamic pricing scheme," *Energies*, vol. 13, no. 8, p. 1950, Apr. 2020. [Online]. Available: https://www.mdpi.com/1996-1073/13/8/1950

[28] M. Shin, D.-H. Choi, and J. Kim, "Cooperative management for PV/ESS-enabled electric vehicle charging stations: A multiagent deep reinforcement learning approach," *IEEE Trans. Ind. Informat.*, vol. 16, no. 5, pp. 3493–3503, May 2020.

[29] Y. Cao et al., "An optimized EV charging model considering TOU price and SOC curve," *IEEE Trans. Smart Grid*, vol. 3, no. 1, pp. 388–393, Mar. 2012.

[30] M. Musio and A. Damiano, "A simplified charging battery model for smart electric vehicles applications," in *Proc. IEEE Int. Energy Conf. (ENERGYCON)*, May 2014, pp. 1357–1364.

[31] J. Han, J. Park, and K. Lee, "Optimal scheduling for electric vehicle charging under variable maximum charging power," *Energies*, vol. 10, no. 7, p. 933, Jul. 2017. [Online]. Available: https://www.mdpi.com/1996-1073/10/7/933

[32] N. Korolko and Z. Sahinoglu, "Robust optimization of EV charging schedules in unregulated electricity markets," *IEEE Trans. Smart Grid*, vol. 8, no. 1, pp. 149–157, Jan. 2017.

[33] C. Shao, X. Wang, X. Wang, C. Du, and B. Wang, "Hierarchical charge control of large populations of EVs," *IEEE Trans. Smart Grid*, vol. 7, no. 2, pp. 1147–1155, Mar. 2016.

[34] H. Turker, A. Hably, S. Bacha, and D. Chatroux, "Rule based algorithm for plug-in hybrid electric vehicles (PHEVs) integration in residential electric grid areas," in *Proc. IEEE PES Innov. Smart Grid Technol. (ISGT)*, Jan. 2012, pp. 1–7.

[35] Z. Wang, P. Jochem, and W. Fichtner, "A scenario-based stochastic optimization model for charging scheduling of electric vehicles under uncertainties of vehicle availability and charging demand," *J. Cleaner Prod.*, vol. 254, May 2020, Art. no. 119886. [Online]. Available: https://www.sciencedirect.com/science/article/pii/S0959652619347560

[36] L. Gan, A. Wierman, U. Topcu, N. Chen, and S. H. Low, "Real-time deferrable load control: Handling the uncertainties of renewable generation," in *Proc. 4th Int. Conf. Future energy Syst.*, May 2013, pp. 113–124.

[37] R. Zdunek, A. Grobelny, J. Witkowski, and R. I. Gnot, "On–off scheduling for electric vehicle charging in two-links charging stations using binary optimization approaches," *Sensors*, vol. 21, no. 21, p. 7149, Oct. 2021.

[38] M. Aziz and T. Oda, *Load Leveling Utilizing Electric Vehicles Their Used Batteries*, M. A. Fakhfakh, Ed. Rijeka, Croatia: IntechOpen, 2016, doi: 10.5772/64432.

[39] E. D. Kostopoulos, G. C. Spyropoulos, and J. K. Kaldellis, "Real-world study for the optimal charging of electric vehicles," *Energy Rep.*, vol. 6, pp. 418–426, Nov. 2020. [Online]. Available: https://www.sciencedirect.com/science/article/pii/S2352484719310911

[40] A. Rahmoun and H. Biechl, "Modelling of Li-ion batteries using equivalent circuit diagrams," *Przeglad Elektrotechniczny*, vol. 88, no. 7, pp. 152–156, 2012.

[41] V. H. Johnson, "Battery performance models in ADVISOR," *J. Power Sources*, vol. 110, no. 2, pp. 321–329, 2002. [Online]. Available: https://www.sciencedirect.com/science/article/pii/S0378775302001945

[42] Q. Lin, J. Wang, R. Xiong, W. Shen, and H. He, "Towards a smarter battery management system: A critical review on optimal charging methods of lithium ion batteries," *Energy*, vol. 183, pp. 220–234, Sep. 2019. [Online]. Available: https://www.sciencedirect.com/science/article/pii/S0360544219312605

[43] E. Inoa and J. Wang, "PHEV charging strategies for maximized energy saving," *IEEE Trans. Veh. Technol.*, vol. 60, no. 7, pp. 2978–2986, Sep. 2011.

[44] A. Tomaszewska et al., "Lithium-ion battery fast charging: A review," *eTransportation*, vol. 1, Aug. 2019, Art. no. 100011. [Online]. Available: https://www.sciencedirect.com/science/article/pii/S2590116819300116

[45] M. Grant and S. Boyd. (2014). *CVX: MATLAB Software for Disciplined Convex Programming, Version 2.1*. [Online]. Available: http://cvxr.com/cvx/

[46] M. ApS, "Mosek optimization toolbox for MATLAB," *User's Guide Reference Manual, Version*, vol. 4, p. 1, Sep. 2019.

[47] G. Fournier, "Design and implementation of a real-life peak shaving charge manager for an electric school bus fleet," in *Proc. 33rd Electr. Vehicle Symp. (EVS)*, Portland, OR, USA, 2020, pp. 1–12.

[48] O. Frendo, N. Gaertner, and H. Stuckenschmidt, "Real-time smart charging based on precomputed schedules," *IEEE Trans. Smart Grid*, vol. 10, no. 6, pp. 6921–6932, Nov. 2019.

[49] I. S. Bayram and I. Papapanagiotou, "A survey on communication technologies and requirements for internet of electric vehicles," *EURASIP J. Wireless Commun. Netw.*, vol. 2014, no. 1, p. 223, Dec. 2014.

[50] SIKA, "RES 2005–2006 the national travel survey," Tech. Rep. 2007:19, 2007.

[51] R. Fachrizal and J. Munkhammar, "Improved photovoltaic self-consumption in residential buildings with distributed and centralized smart charging of electric vehicles," *Energies*, vol. 13, no. 5, p. 1153, Mar. 2020. [Online]. Available: https://www.mdpi.com/1996-1073/13/5/1153

[52] M. Lahariya, D. F. Benoit, and C. Develder, "Synthetic data generator for electric vehicle charging sessions: Modeling and evaluation using real-world data," *Energies*, vol. 13, no. 16, p. 4211, Aug. 2020. [Online]. Available: https://www.mdpi.com/1996-1073/13/16/4211

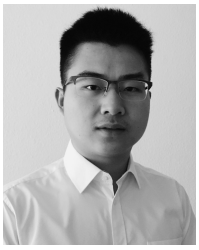

Kun Qian received the B.Sc. degree from Hangzhou Dianzi University, Hangzhou, China, in 2016, and the M.Sc. degree from the University of Southern Denmark, Sønderborg, Denmark, in 2018, where he is currently pursuing the Ph.D. degree.

His current research interests include electric vehicles' charging infrastructure and scheduling.

Reza Fachrizal received the B.Sc. degree in electric power engineering from the Bandung Institute of Technology, Bandung, Indonesia, in 2015, and the M.Sc. degree in renewable electricity production from Uppsala University, Uppsala, Sweden, in 2018, where he is pursuing the Ph.D. degree in engineering sciences with the Department of Civil and Industrial Engineering.

His research interests are related to the synergy between photovoltaic generation and electric vehicle charging load in the built environment.

Joakim Munkhammar received the Ph.D. degree in engineering sciences from Uppsala University, Uppsala, Sweden, in 2015.

He is currently an Associate Professor of civil engineering at Uppsala University. His research is focused on mathematical energy modeling into solar energy, mobility, and energy use in buildings.

Thomas Ebel (Senior Member, IEEE) received the Dipl.-Chem. degree (M.Sc. equivalent) in Chemistry from Münster University, Münster, Germany, in 1992, and the Ph.D. degree (Dr. rer. nat.), from the Institute of Inorganic Chemistry, Münster University, in 1995.

In 1995, he spent three months as a Guest Researcher at the CNRS, Institute des Matériaux de Nantes, Nantes, France, with Prof. J. Rouxel. From August 1995 to September 2001, he was a Research and Development Engineer and later the Research and Development Director at Siemens Matsushita Components, Siemens AG PR, since October 1999 EPCOS AG, since October 2008 TDK, in the Business unit of Aluminum- Electrolytic- Capacitors, Heidenheim, Germany. From October 2001 to July 2008, he was the Research and Development Director, later the Technical Director (CTO), the Member of the Board of Directors at Becromal Norway (Becromal S.p.A, since October 2008 Epcos, now TDK foil), Milano, Italy. From September 2008 to July 2018, he was the Managing Director and Shareholder at FTCAP GmbH, Husum Manufacturer of Aluminum Electrolytic and Film-Capacitors, Heidenheim. Since August 2018, he has been the Head with the Section Electrical Engineering and Centre for Industrial Electronics (CIE), Odense, Denmark and University of Southern Denmark (SDU), Sønderborg, Denmark. He has a rank of a Full Professor.

Rebecca C. Adam received the Dipl.-Ing. degree (M.Sc. equivalent) in electrical engineering and information technology from Kiel University, Kiel, Germany, in 2009, and the Ph.D. degree (Dr.Ing.) from the Chair for Information and Coding Theory, Kiel university, in 2021.

From 2009 to 2016, she was a Research Assistant at the Chair for Information and Coding Theory, Kiel university, including two years of maternity leave. From 2018 to 2019, she worked as a Software Developer in industry. Since 2019, she has been working as a Research Assistant, as a Post-Doctoral Researcher, and as an Assistant Professor at the Centre for Industrial Electronics, University of Southern Denmark, Sønderborg, Denmark. Her research interests include optimization, estimation theory, and machine learning applied to areas of electric vehicle fleet charging systems, and wireless communication.

Dr. Adam was a recipient of the Best Paper Award at the 10th Workshop on Positioning, Navigation and Communication (WPNC) 2013.